Transport

Analysis of the performance of under-sleeper pads in high-speed line transition zones
Insa, Salvador, Inarejos and Medina

ice | proceedings

Proceedings of the Institution of Civil Engineers

http://dx.doi.org/10.1680/tran.11.00033
Paper 1100033
Received 24/06/2011 Accepted 11/04/2012
Keywords: dynamics/mathematical modelling/rail track design/railway systems

ice Institution of Civil Engineers publishing

Analysis of the performance of under-sleeper pads in high-speed line transition zones

1 **Ricardo Insa** PhD
Professor, Department of Transport Engineering and Infrastructure, Polytechnic University of Valencia, Valencia, Spain

2 **Pablo Salvador** MEng
Researcher, Department of Transport Engineering and Infrastructure, Polytechnic University of Valencia, Valencia, Spain

3 **Javier Inarejos** MEng
Researcher at the Department of Transport Engineering and Infrastructure, Polytechnic University of Valencia, Valencia, Spain

4 **Luis Medina** PhD
Assistant Professor, Department of Geotechnical Engineering, University of La Coruña, La Coruña, Spain




In many high-speed railway lines, the zones between embankments and structures may present some discontinuities, in terms of track geometry and track stiffness, which may create discomfort for passengers, induce deterioration of track and vehicle materials and even raise the risk of derailment to dangerous levels. In the attempt to attenuate the consequences of such problems, some solutions pointing at progressively changing the vertical stiffness in the railway track have been tested, such as transition zones or pads placed either between the rails and the sleepers or under the sleepers. The contribution of under-sleeper pads in transition regions and their effect on the railway infrastructure is specifically analysed in the present paper. The results obtained are of interest since they provide useful information for railway managers on infrastructure design and justify the need to implement such transition zones.

Notation

b	maximum vertical alignment measured with a chord length of 3 m
c	cohesion
c_1	track global damping
c_2	primary suspension damping
c_3	secondary suspension damping
E	Young's modulus of rail
I	rail moment of inertia
k_1	track global vertical stiffness (constant)
$k_1(s)$	track global vertical stiffness (variable with length)
k_2	primary suspension stiffness
k_3	secondary suspension stiffness
L	distance between sleepers
L_m	total length of the model
M_{us}	unsprung masses per wheelset
m_1	wheelset mass
m_2	bogie frame mass
m_3	car body mass
Q	vertical static load induced by a wheelset
Q_{dyn}	dynamic loads
Q_n	static load
s_0	initial position of the train
t	time
u, v, w	displacements in the x, y and z directions
V	speed of the train
x, y, z	axis directions
z	rail profile
γ	specific weight
$\varepsilon(s)$	track settlement at the track point s
ν	Poisson's ratio
ρ	vertical track stiffness
σ_s	sprung masses
σ_s	unsprung masses
ϕ	internal angle of friction

1. Introduction

Transition regions may become a serious handicap for high-speed railway operations and maintenance work. The fact that the stretches of the tracks built on embankments can undergo larger settlements than those placed over structures such as bridges, tunnels or transverse drainages may cause a noticeable discontinuity in the track geometry. Due to the huge dynamic forces between the train and the tracks that are induced by these geometric discontinuities, it may be necessary to set up temporary speed restrictions which hinder the normal railway operations. In addition, such discontinuities need continuous maintenance work, raising the maintenance costs to levels that are sometimes unacceptable.

In order to limit the abrupt change between settlements on embankments and structures, so-called 'transition regions', 'transition wedges' or 'transition zones' are built between these two infrastructure parts, and consist in increasing track vertical stiffness by building the embankments with stiffer materials such as granular soils and hydraulic soils as they approach the structures. Nevertheless, in some cases, the change in the track geometry is too sharp even with the use of transition regions, which can be due to incorrect construction techniques or inappropriate soil foundations.

The problem of transition regions has not been properly analysed despite its significance. One study set up a dynamic model which is divided into two parts and solved independently through an iterative scheme (Lei and Mao, 2004). The upper structure is the train, which includes the vertical and pitch motion for the carriage and the bogies. The lower structure is the railway track, where the rails are considered as beams resting on a double-layer elastic foundation. Other research analysed track transitions from a portal frame bridge point of view, principally as a structural problem (Ülker-Kaustell *et al.*, 2010). Other work reported a case study on two railway bridge transitions against heavy freight trains (Hyslip *et al.*, 2009). However, these studies were limited to direct changes from embankments to structures, so transition regions were not analysed, and the dynamic load inputs in the studies of Lei and Mao and of Hyslip *et al.* were for trains whose speed was lower than 160 km/h, which differ from high-speed train dynamic loads. Other studies also analysed transition regions as a means to smooth the wheel–rail impact of a train when passing from a floating slab track to a ballasted track (Li and Wu, 2009).

From the infrastructure point of view, a finite-element model, whose most distinctive characteristic is its attempt to simulate the real behaviour of the diverse materials which make up the structure of the track in a transition, was developed (Gallego and López Pita, 2009). The study considered the surface defining the embankment slope as free and took into account the elastoplastic behaviour of the soil. More comprehensive research regarding different situations involving changes of vertical stiffness suggested some solutions for smoothing them, such as the use of under-sleeper pads (USP) or grouting (Burrow *et al.*, 2010; Dahlberg, 2010).

Smoother changes in the track vertical stiffness can also be achieved by varying the elastic properties of resilient pads incorporated into the track structure. These pads are normally placed between the rails and the sleepers, although there are some other kinds of pads which can be placed either under the sleepers or under the ballast. Studies involving pads of the first type were focused on a sensitivity analysis of free vibration characteristics of an in situ railway concrete sleeper to variations of rail pad parameters (Kaewunruen and Remennikov, 2006); and on setting up an alternative for railpad testing allowing for the measurement of stiffness and damping values for frequencies between 20 and 2500 Hz with variable preload (Maes *et al.*, 2006).

The influence of USPs on the dynamic train–track interaction was analysed in a parametric study (Johansson *et al.*, 2008) in which a USP dynamic modulus three times greater than the static modulus is considered. Johansson's paper has three main conclusions: that the UPS only influences the lower part of the frequency spectrum (<250 Hz); that the highest rail pad stiffness in combination with the lowest USP stiffness yields the highest acceleration; and that the railseat loads are almost independent of the USP stiffness.

Wang *et al.* (2008) proposed a study on rubber-modified asphalt concrete acting as ballast mats which are modelled following a hysteretic behaviour, whereas Hanson and Singleton (2006) used a simple single-degree-of-freedom model developed by Wettschureck and Kurze (1985). Comparisons between predictions and measurements indicate good agreement for the resonant frequency dip and the mid-frequency insertion loss.

The aim of the work reported here is to analyse and discuss the use of under-sleeper pads in transition zones and their impact on the railway infrastructure. The research is firstly focused on the effect of the train passing over the infrastructure, in terms of displacements and stresses throughout its different parts. The analysis has been carried out by means of 3D numeric modelling using the finite-difference method, implemented by means of the FLAC 3D software. Additionally, in order to analyse the effect of the track-deformed geometry on the train, a three-degrees-of-freedom dynamic model has been set up, which allows calculation of the passenger car accelerations and the wheel–rail contact force, among other variables. The equations of this model are also solved numerically by the finite-difference method. The necessary data for setting up the models come from the Valencia–Játiva High-Speed Line Project and the trainsets which currently run from Madrid to Valencia.

This paper is structured as follows: first, a deeper description of the dynamic problem existing in transition zones is given, as well as the behaviour of under-sleeper pads. Second, the procedure employed in the modelling performing static calculations is commented on, together with the different superstructure configurations. Then, the results of the calculations are discussed in terms of displacements, stresses and sensitivity analysis of different parameters. In the next part, the dynamic model is presented, explaining its most relevant features and commenting on the results obtained. Finally, some concluding remarks are given and recommendations concerning the use of under-sleeper pads in transition regions are proposed.

2. The problem in the transition zones

Changes in track vertical stiffness cause an increment of dynamic forces, whose magnitude is determined by the speed of the trains, the ratio between stiffnesses, the soil damping and the transition length. Furthermore, differential settlements on tracks lead to a significant increment of accelerations in the vehicles, which cannot achieve the passenger comfort levels or the maximal

dynamic forces allowed by the tracks. Such magnification of vertical forces produces track deterioration and increases infrastructure maintenance costs (Esveld, 2001).

In order to reduce this damaging effect, transition zones or transition wedges are built between sections with different stiffnesses – for example, embankments and structures, as mentioned in Section 1. In this way, a smoother deformation is achieved through the different sections of the transition, so that the increment of stiffness is achieved progressively before reaching the structure. Figure 1 shows the schematic solution offered in the recommendations for railway infrastructure plans in Spain IGP 2008 (Adif, 2008) and a typical location of this zone.

It is also possible to change the most rigid zones, normally acting over the abutment or the deck of the bridge, by setting up elastic materials either between the sleepers and the ballast or between the ballast and the structure. Logically, a combination of the measures described above is also suitable.

Of all the possible solutions, USPs have the advantage of contributing to a better redistribution of stresses in the lower layers of ballast tracks by increasing the contact surface area, lowering transmitted stresses and thus preserving the ballast layer. This is due to the lower stiffness of USPs compared with concrete sleepers, so that the contact between the bottom of the sleepers and the ballast does not become sharp-edged.

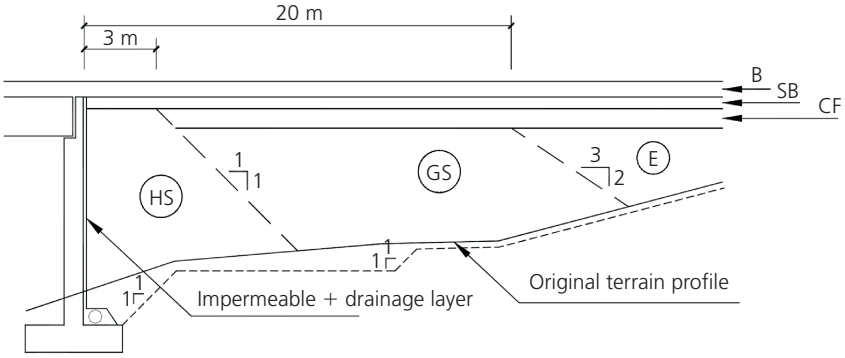

(a)

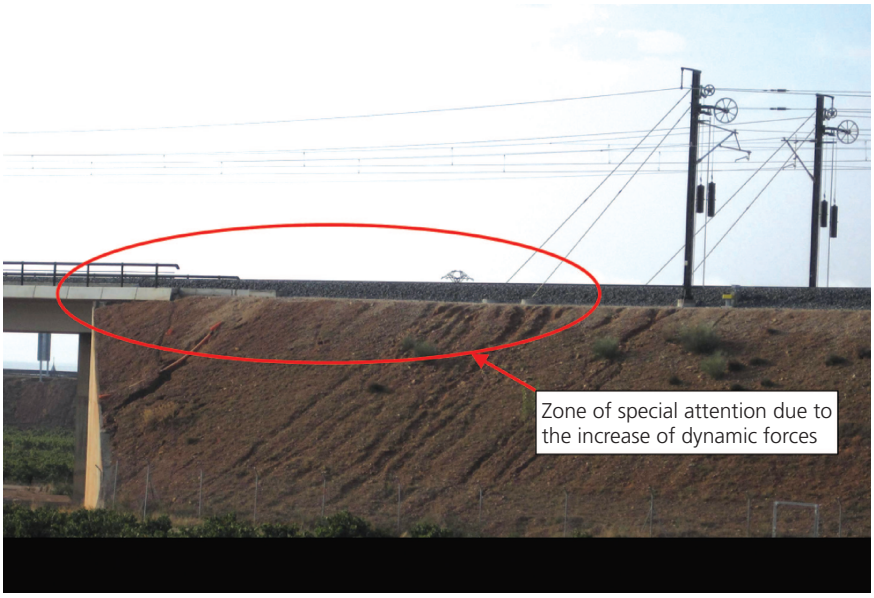

(b)

Figure 1. (a) Schematic profile of an embankment–bridge transition zone proposed by Adif. HS, hydraulic soil; GS, granular soil; E, embankment; B ballast layer; SB, sub-ballast layer; CF, form layer. (b) Transition zone built between an embankment and a bridge in the Madrid–Valencia high-speed line

3. Static model description

This model represents the behaviour of a transition region and its different component materials when the loads induced by a train are applied. The modelled railway section corresponds to a double-track high-speed line from the Valencia–Játiva stretch. The model, shown in Figure 2, includes the different materials which compose the transition (the embankment, the granular soil, the hydraulic soil and the form layer) as well as the different track materials (the sub-ballast, the ballast, the under-sleeper pads, the sleepers, the pads and the rails). No possibility of deformation was considered for the concrete structure, so it is modelled as boundary conditions. The length of the grid is 43·2 m, corresponding to 38·4 m in the soil zone and 4·8 m in the concrete structure.

In the reference system chosen, the x-axis coincides with the backward direction of the train; that is, the distance to the origin decreases as the train approaches the structure; the z-axis coincides with the vertical direction, being positive upwards; and the y-axis coincides with the sleepers' direction, being positive inwards. In this way, a right-turn reference system is obtained. The origin is placed at the bottom, immediately below the track axis, in the plane that separates the hydraulic soil and the structure. Due to the symmetry of the problem, only one track is modelled.

The thicknesses of the different layers are 6·0 m for the embankment, 0·5 m for the form layer, 0·3 m for the sub-ballast and 0·35 m for the ballast. It must be noted that the form layer is not built over the hydraulic soil, which is directly in contact with the sub-ballast, as specified in IGP 2008 (Adif, 2008).

The sleepers are concrete monoblock type and their weight is approximately 300 kg. The rails are UIC-60, whose modelling consisted of equivalent rectangular beams with the same cross-sectional inertia as the original rails. The rail pads are 7 mm high

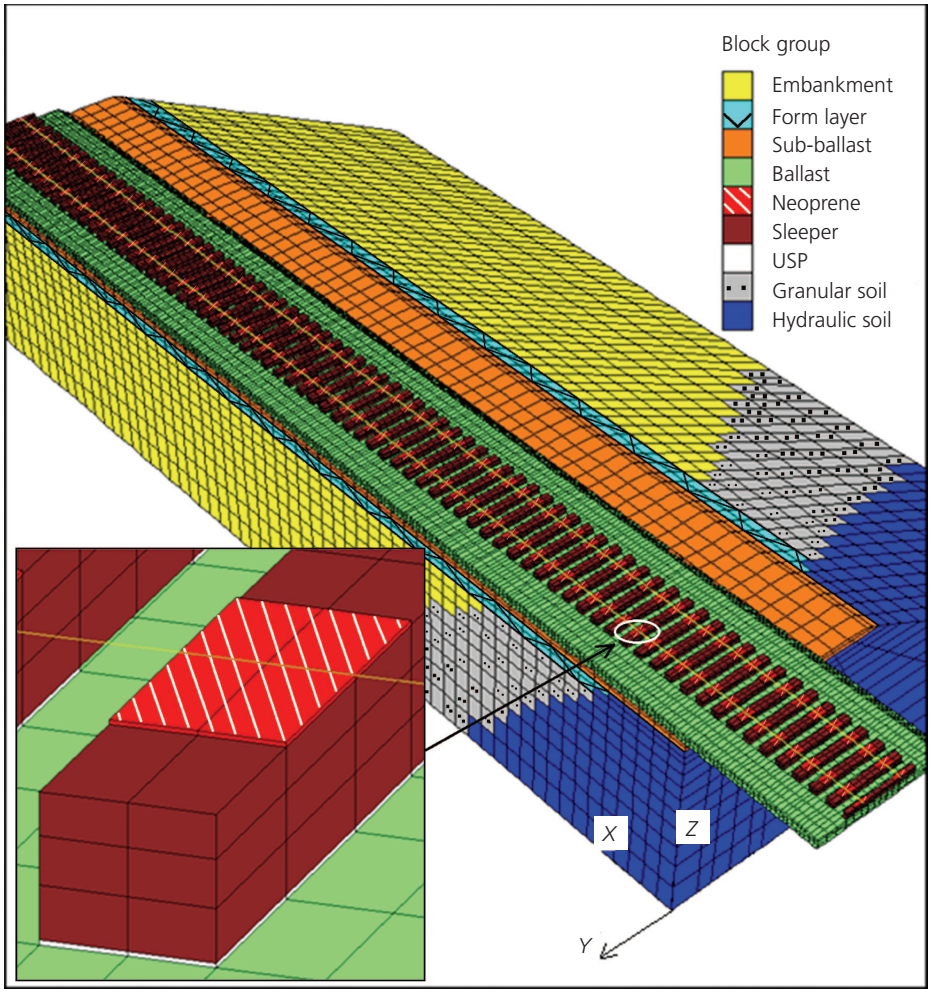

Figure 2. View of the whole model with the Cartesian axes adopted and detail of the under-sleeper pads (USPs)

and their elasticity modulus was determined from the neoprene stiffness (10^8 kN/m), their height and the contact surface with the rails. For USPs, the same properties as for the rail pads are assumed initially, although these properties were modified during the sensitivity analysis.

The boundary conditions applied are

(*a*) plane $y = 0$ (symmetry plane): $v = 0$
(*b*) plane $x = L_m$: $u = 0$
(*c*) plane $z = 0$ (base of the grid): $w = 0$
(*d*) plane $x = 0$ (beginning of the structure): $u = 0$
(*e*) plane $x = -4{\cdot}8$ (beginning of the grid): $u = 0$
(*f*) plane $z = 6{\cdot}8|_{x<0}$ (horizontal plane under the ballast in the part of the structure): $v = 0$, $w = 0$

where $\{x, y, z\}$ are the different axis directions, $\{u, v, w\}$ are the displacements in the x, y and z directions, respectively, and L_m is the total length of the model.

The constitutive models adopted are linear elastic for the sleepers, the rail pads, the under-sleeper pads and the rails; and Mohr–Coulomb elastoplastic for the rest of the materials. The properties of the materials are shown in Table 1, where E is the elasticity modulus, ν is the Poisson ratio, c is the cohesion, ϕ is the internal angle of friction and γ is the specific weight. The values have been extracted from Ministerio de Fomento (1999), Esveld (2001) and Profidillis (1983).

The model grid consists of some 27 400 elements and 39 100 nodes. The calculation process requires about 4 h on a Pentium IV 3·6 GHz and 2 GB RAM.

4. Analysis and results with the static model

4.1 Displacements analysis

The settlements produced by a real train in the model described above are first determined. Since this is a static analysis, the movement of the train is not considered.

The train consists of a locomotive plus the adjacent car. From this configuration, the real train can be obtained by adding more cars, but since all cars have similar dimensions and weights, it is not worthwhile modelling the whole train. Furthermore, a model considering the entire train would take weeks to solve, which is not acceptable in practice.

The loads' position is as follows: the train goes towards the structure and the front wheels of the locomotive are located 0·5 m before the structure. The distance between bogies on the locomotive is 11 m and the distance between the axles in the bogies is 2·65 m. The distance between the centre of the bogie and the first axle of the adjacent car is 5·475 m and the distance between the car axles is 13·14 m, except for the adjacent car to the locomotive, for which it is 10·52 m.

The train static loads have been increased in order to consider the dynamic effects of the train–track interaction using the Prud'Homme formula (Prud'Homme, 1970). This formula calculates the total load as the sum of the static load Q_n plus an increment due to the dynamic load Q_{dyn}.

$$1. \quad Q_t = Q_n + Q_{dyn}$$

Dynamic loads are estimated by the standard deviation they produce.

$$2. \quad \sigma = \sqrt{(\sigma_{us}^2 + \sigma_s^2)}$$

where σ is the standard deviation due to the dynamic effects; σ_{us} is the contribution of the unsprung masses (i.e. those masses directly in contact with the rail) and is given by

$$3. \quad \sigma_{us} = 0{\cdot}0042bV\sqrt{\left(\frac{M_{us}\rho}{10}\right)}$$

Material	E: kPa	ν	c: kPa	φ: degrees	γ: kN/m^3
Embankment	$4{\cdot}0 \times 10^4$	0·30	15	30	17·3
Form layer	$8{\cdot}0 \times 10^4$	0·30	0	35	16·0
Granular soil	$8{\cdot}0 \times 10^4$	0·30	0	30	17·3
Hydraulic soil	$16{\cdot}0 \times 10^4$	0·30	20	35	17·3
Sub-ballast	$12{\cdot}0 \times 10^4$	0·30	0	35	16·0
Ballast	$13{\cdot}0 \times 10^4$	0·20	0	45	16·0
Concrete sleeper	$5{\cdot}0 \times 10^7$	0·25	—	—	24·0
Rails	$2{\cdot}1 \times 10^8$	0·30	—	—	78·0
Rail pads	$7{\cdot}5 \times 10^4$	0·45	—	—	20·0
Under-sleeper pads	$7{\cdot}5 \times 10^4$	0·45	—	—	20·0

Table 1. Mechanical parameters of the various materials

where b is the maximum vertical alignment measured with a chord length of 3 m, in mm; V is the speed of the train in km/h; M_{us} is the unsprung masses per wheelset, in tonnes; and ρ is the vertical track stiffness, in kN/mm.

The contribution of the sprung masses – that is, those masses placed above the primary suspension – is σ_s, which is calculated as a part of the static load

$$\sigma_s = \alpha Q_n \quad (4)$$

with α ranging from 0·11 to 0·16.

Assuming a statistical factor of 2, the dynamic load Q_{dyn} is obtained as twice the standard deviation of dynamic loads σ. In this way, Figure 3 shows the train load distribution together with the increased load values. The necessary data for deriving such load values are shown in Table 2.

With all these conditions, the longitudinal profiles of the deflections experienced by the rails and the different layers which compose the whole infrastructure are shown in Figure 4, where the settlements correspond to the upper plane of each layer. In this figure, the different vehicles and loads applied in the model can be appreciated. The track deflections over the structure can be neglected. Starting from the structure and following the positive direction of the x-axis, the two peaks corresponding to the front bogie can be identified first. After these, the peaks from the rear bogie appear. Then comes the front wheel of the adjacent car, and finally the rear wheel of this car.

The differences between the settlements corresponding to the cases with USPs and without them are practically nil. This was expected because the thickness of the USPs is very small compared with the rest of the materials' thickness. Consequently, their deformation contributes weakly to the deformation of the whole infrastructure.

The settlement levels through the different layers are not modified by the placing of the pads under the sleepers. Only in the zone of contact of the sleepers with the ballast does a slight difference exist due to the fact that the sleepers with no pads have their entire lower side as the contact surface, whereas in the case with pads, only the area of the pads is in contact with the ballast. In this way, the settlements under the sleepers are slightly greater in the case with pads, as can be noted in Figure 5.

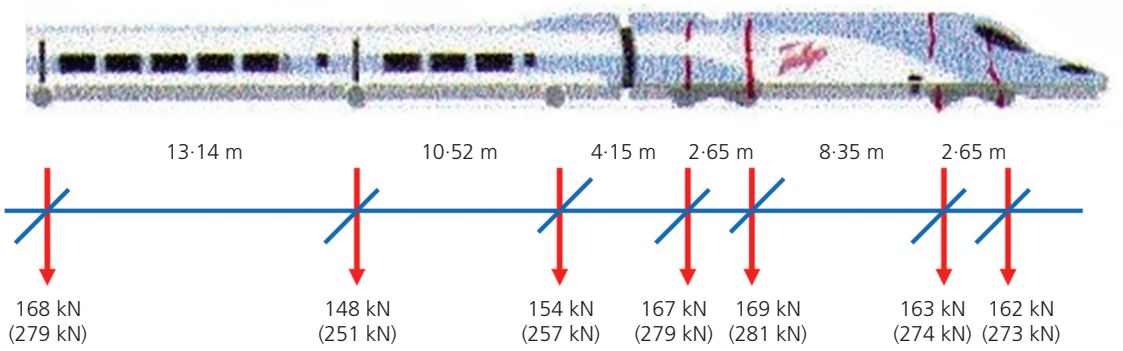

Figure 3. Static load distribution produced by the train. The values in brackets are the increased values given by Prud'Homme's formulation

V: km/h				300			
b: mm				1			
ρ: kN/mm				100			
Wheelset number	1	2	3	4	5	6	7
Wheelset static load: kN	162	163	169	167	154	148	168
M_{us}: t	1·50	1·50	1·50	1·50	1·42	1·42	1·42
M_s: t	15·01	15·12	15·73	15·52	14·28	13·67	15·71
α	0·16	0·16	0·16	0·16	0·13	0·13	0·13
Wheelset increased load: kN	272·99	274·14	281·09	278·77	257·36	250·74	272·88

Table 2. Input parameters and results for the increased quasi-static load provided by Prud'Homme's formulation

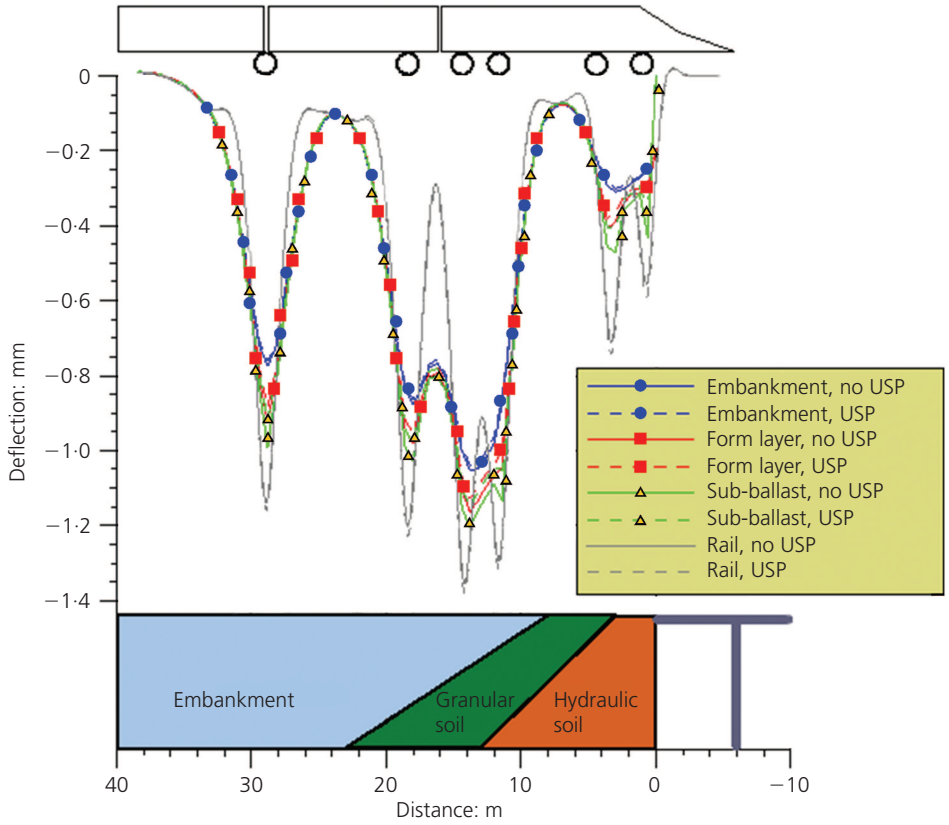

Figure 4. Longitudinal profile for the deflections in the rails and in the different layers which compose the infrastructure

The rationale of this model is to reflect the most severe working condition in the long term, in which the sleepers with no USPs have settled on the ballast, thus transmitting the loads through the entire lower surface and not through the areas placed under the rails as is expected. Since the USPs also help to keep the initial stress distribution under the sleepers, they have been represented as two separated pieces placed in the zone under the rails instead of totally covering the lower surface of the sleepers. This slightly increases both settlements and stresses transmitted to the lower layers of the infrastructure, but makes the sleepers work under the conditions they were designed for.

4.2 Stress analysis

In this subsection, stress distribution throughout the model is analysed. Figure 6 shows the variation of vertical stresses with depth. For better understanding of the distribution of stresses, the different layers of the infrastructure are also shown. The curve with circles represents the in situ state of stresses; the curve with squares is the sum of the previous curve plus the stresses produced by the train; and the curve with no data symbols, the most interesting one, reflects the stresses produced exclusively by the train.

The main part of the load applied by the train is absorbed by the ballast lowering the initial loads, which range in the upper plane between 47 kPa when not using USPs and 60 kPa when using them, down to approximately 20 kPa in the lower plane for both cases. In a similar way as with the deformations, the stresses immediately under the pads are greater than in the case when no pads are installed because the contact surface is smaller in the first case than in the second. These results correspond to the cross-section located 14 m before the structure, immediately underneath the inner rail. In the layers below the ballast, there is no appreciable difference in the stresses between the two situations.

4.3 Sensitivity analysis

A sensitivity analysis was carried out by varying the following parameters: the elasticity modulus of the USPs in the first instance and the thickness of the USPs in the second. Together with this, two different cases were evaluated: placing USPs under all the sleepers or placing them only under those sleepers located in the structure. In addition, the potential scenario of removing transition regions and leaving only USP was also analysed.

Following the procedure employed in the previous analysis, a uniform static load was applied along the rails, whose magnitude produces a constant deflection similar to that produced by the train far from the transition region. In this specific case, a load producing a uniform deformation of 1 mm was considered, a

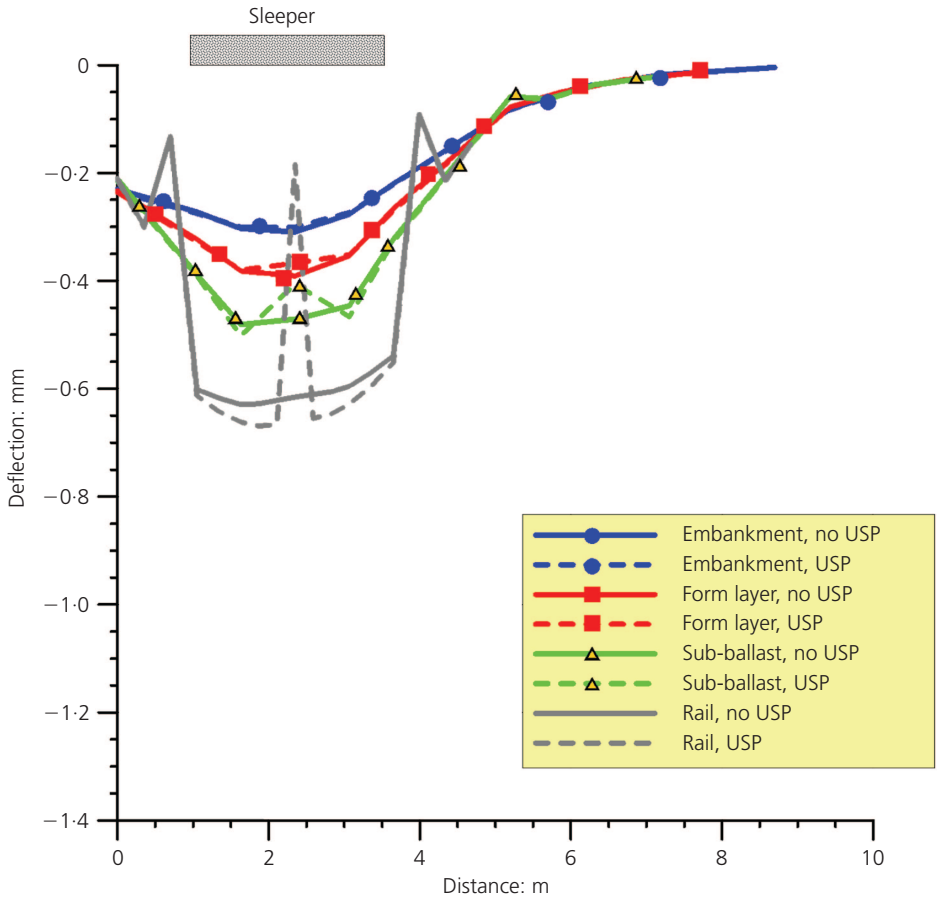

Figure 5. Transversal profile for the settlements in the different materials which compose the infrastructure. Section taken 14 m from the beginning of the structure

slightly smaller value than the settlement induced in the rail immediately under the wheel – approximately 1·3 mm. As the present analysis deals with high speeds (greater than 100 km/h), it is reasonable that the deflection profile of the rails when the train is passing over the transition zones is more similar to that produced by a constant load (of the kind supposed at this point) than to the static-shaped curve shown in Figure 3. Thus as a starting point for calculations, it is considered that the vertical path followed by the train is similar to the deflection curves obtained at this point caused by a constant load along the rails.

First, the elasticity modulus of the USPs was varied from 7500 kPa (one order of magnitude smaller than the modulus of the rail pads) to 150 000 kPa (twice the stiffness of the rail pads). The results obtained are shown in Figure 7, where the lack of influence of this parameter in the rail settlement can be appreciated. Second, the USP thickness was modified, varying from 4 mm to 20 mm, although the maximum thickness recommended for this material is 15 mm. The results are shown in Figure 8, and no significant influence of this parameter can be noted.

In addition, the effectiveness of USPs for smoothing the settlement profile was tested. Since the structure is much stiffer than the embankment, in order to diminish the difference between the stiffnesses, the pads were placed only under the sleepers located on the structure. For this analysis, the elasticity modulus of the USP was varied as shown in Figure 7, and the results are shown in Figure 9. Once more, no appreciable difference is found. There is only a slight difference in the settlements in the embankment part, which is due to a transfer of the bending moments from the structure.

Finally, the possibility of removing transition regions when USPs are employed was studied. For this, two different situations were considered: first, the elasticity modulus of the USPs was modified as shown in Figure 7; second, the thickness of the USPs was varied as shown in Figure 8. The results are shown in Figure 10 only for the case of varying USP stiffness, since the results for the second case are practically identical to those obtained for the first. In this figure, the rail deflection as the track reaches the structure from the embankment is sharper than in the case of using transition regions, and once again no significant influence of the USP elasticity or the USP thickness is detected.

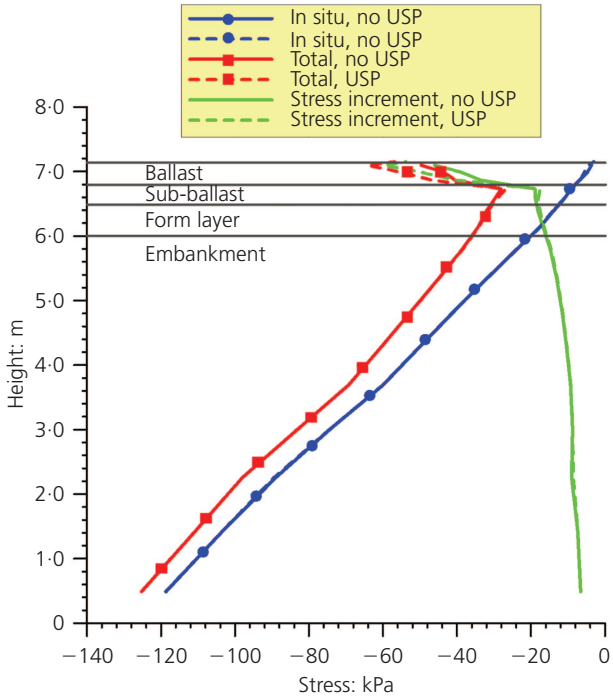

Figure 6. Distribution of vertical stresses under the inner rail with respect to the depth. Section taken 14 m from the beginning of the structure

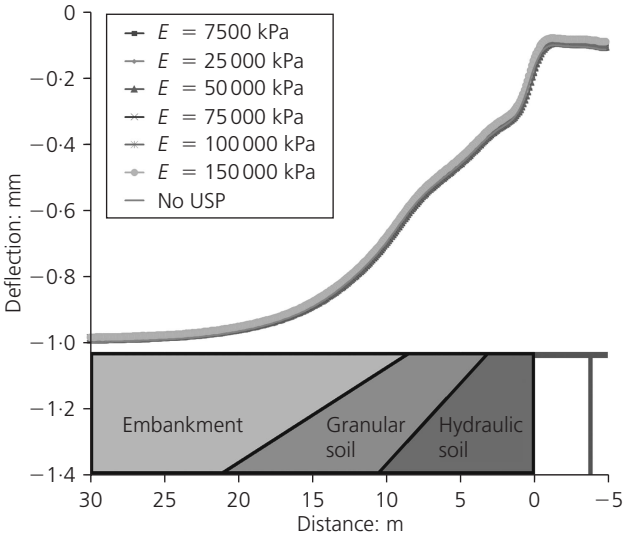

Figure 7. Different longitudinal profiles of deflections with varying elasticity modulus of the USP

5. Dynamic model description

5.1 Main features and governing equations

In order to analyse the influence on the passengers' comfort, a train–track interaction dynamic model was set up. In the literature there are suitable models in terms of number of degrees of freedom in the vehicle (Baeza *et al.*, 2006) and consideration of the parametric excitation (Wu and Thompson, 2004). For the purpose of this part of the study, a dynamic model with three degrees of freedom is sufficient. Such a model gives a good approach to the vehicle body accelerations while allowing consideration of a varying stiffness along the track and the effect of the parametric excitation.

Figure 11 shows the model, where m_1 represents the mass of half a wheelset, including the axlebox; m_2 represents the mass of a

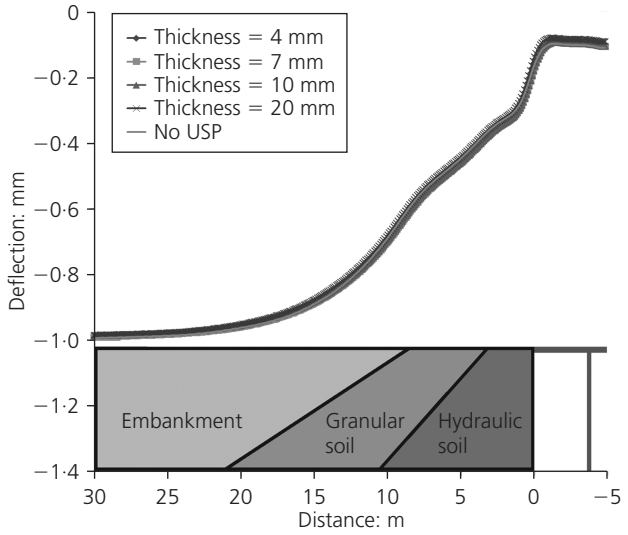

Figure 8. Different longitudinal profiles of deflections with varying thickness of the USP

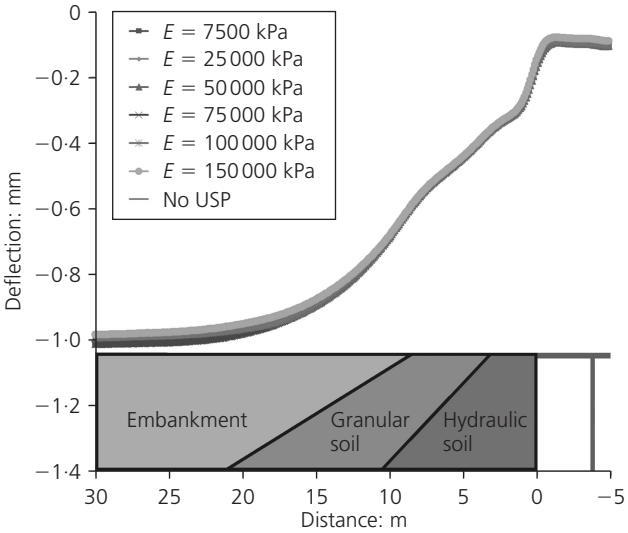

Figure 9. Different longitudinal profiles of deflections with varying elasticity modulus of the USP. USP placed only under the sleeper in the structure

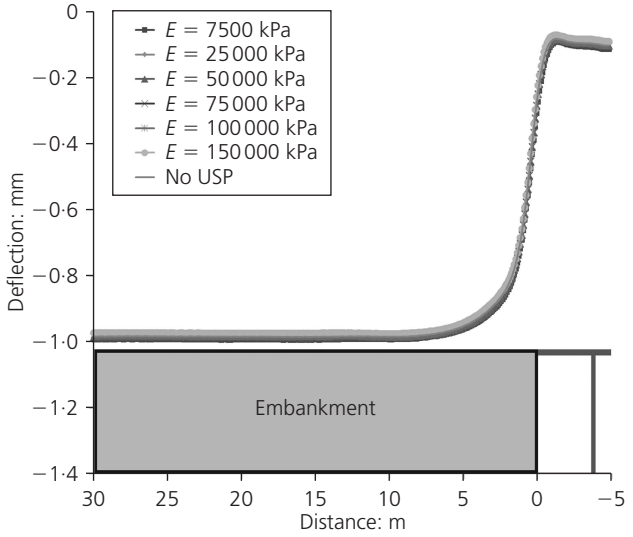

Figure 10. Different longitudinal profiles of deflections with varying elasticity modulus of the USP. No transition region

quarter of a bogie frame; and m_3 represents the mass of an eighth of the vehicle body. In the same way, k_1 and c_1 represent respectively the overall stiffness and damping of the track; k_2 and c_2 represent respectively the stiffness and damping of the primary suspension, as do and k_3 and c_3 for the secondary suspension. The different degrees of freedom correspond to the vertical movements and are denoted by x_1, x_2 and x_3. The rail profile is represented by z. In this way, the model equations are (Melis, 2008)

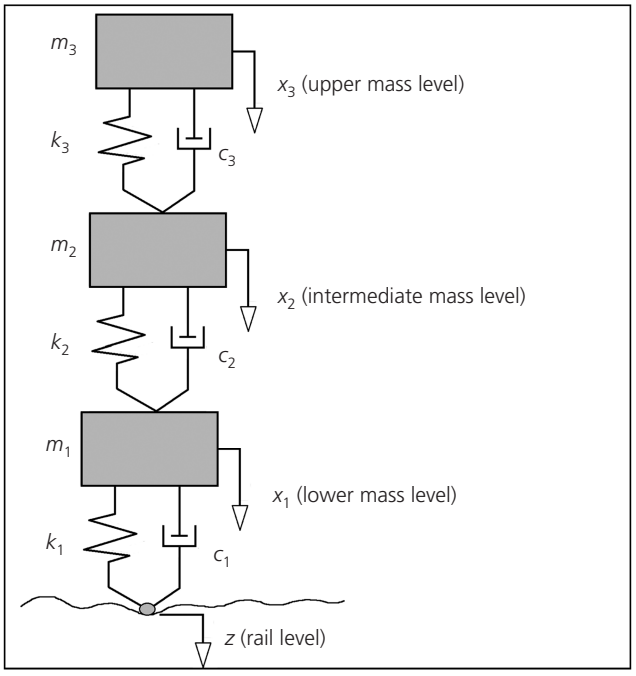

Figure 11. Scheme of the three-masses dynamic model representing the train–track interaction

$$\text{5a.}\quad \ddot{x}_3 = \frac{1}{m_3}[-c_3\dot{x}_3 + c_3\dot{x}_2 - k_3x_3 + k_3x_2]$$

$$\ddot{x}_2 = \frac{1}{m_2}[c_3\dot{x}_3 - (c_3 + c_2)\dot{x}_2 + c_2\dot{x}_1$$

$$\text{5b.}\quad + k_3x_3 - (k_3 + k_2)x_2 + k_2x_1]$$

$$\ddot{x}_1 = \frac{1}{m_1}\{c_2\dot{x}_2 - (c_1 + c_2)\dot{x}_1 + k_2x_2$$

$$\text{5c.}\quad - [k_1(s) + k_2]x_1 + c_1\dot{z} + k_1(s)z\}$$

Notice that in Equation 5c, $k_1 = k_1(s)$ since the track stiffness varies along the track length, defined by s.

The set of equations (5a–c) is solved numerically by the finite-difference method (FDM). No analytic solution is possible, since the coefficient k_1 is not constant. Numeric derivation is achieved by applying the following formulae for the first and second derivatives, respectively (Puy, 1985).

$$\text{6.}\quad f'_0 = \frac{1}{h}(f_1 - f_0) - \frac{h}{2}f^{(2)}(\xi)$$

$$\text{7.}\quad f''_0 = \frac{1}{h^2}(f_{-1} - 2f_0 + f_1) - \frac{h^2}{12}f^{(4)}(\xi)$$

where f'_0 and f''_0 are the first- and the second-order derivatives at the evaluated point, respectively; f_{-1} and f_1 are the values for the deflection at the preceding and the following point, respectively; h is the step between the evaluated points and the second term is the error as a result of the derivation process. The necessary initial boundary conditions for running the model are

$$\text{8a.}\quad x_i(0) = z(0) \qquad i = 1, 2, 3$$

$$\text{8b.}\quad \dot{x}_i(0) = 0 \qquad i = 1, 2, 3$$

whose physical meaning is that all the masses are at their respective equilibrium point with null vertical velocity.

5.2 Calculation of track vertical stiffness

As stated before, the track vertical stiffness $k_1(s)$ varies along the track due to the different material configurations among the

subsequent infrastructure sections, for example the embankment, the transition zone (if placed) and the structure. It is obtained for every point by applying its definition

$$k_1(s) = \frac{Q}{\varepsilon(s)} \tag{9}$$

where Q is the vertical static load induced by a wheelset and $\varepsilon(s)$ is the track settlement at the track point s obtained in the static model explained in Section 3 and whose results are shown in Figures 7 and 10. Such vertical stiffness includes the contribution of the rails, the rail pads, the USP, the ballast and the underlying materials. For this case, only the elasticity modulus of the USP was varied, since the results described in Figure 7 show no significant difference on the thickness variation.

5.3 Calculation of rail vertical profile

The rail vertical profile is obtained taking into account two different issues: the quasi-static load and the parametric excitation. The deformed rail profile caused by the quasi-static load can be obtained by applying a uniform point load of the magnitude of the wheelset load at different points along the model described in Section 3 corresponding to different time instants. The rail profile is thus the envelope of these different rail profiles, provided the point load has been displaced each time with relatively short distance increments. In practice, this method is very time consuming, so the deformed rail profile was chosen as that shown in Figures 7 and 10, assuming the hypothesis of a uniform load which causes a constant rail deflection far from the transition zone, as explained in Section 4.3.

The effect caused by a wheel running on a discretely supported rail is called parametric excitation and causes the unsprung masses of the train not to follow a horizontal path but rather a sinusoid. This is because the rail deflection when the wheel is located exactly above a sleeper is different from that when the wheel is located at the centre of a sleeper bay. In this way, we can consider a wheelset running on a sinusoid whose amplitude is half the difference of both rail deflections.

A method for calculating rail settlements based on a continuous beam resting on discrete elastic foundations was first developed by Unold (1925) and later completed by Dischinger (1942) and Carlos Lorente de Nó (1980). This method allows consideration of the effect of the parametric excitation, depending on the track vertical stiffness, the rail properties, the distance between sleepers and the wheelset load. Figure 12 shows this scheme, in which the track is considered as an Euler–Bernoulli beam discretely resting on linear elastic supports.

The method introduces a parameter λ called 'constant of yielding' which is related to the stiffness of the supports by

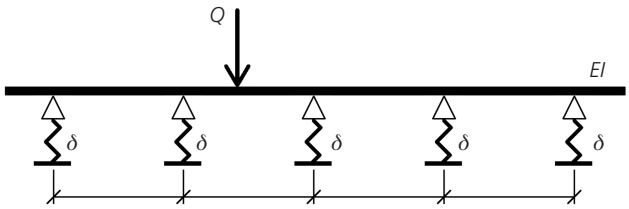

Figure 12. Diagram of a constant moving point load on a beam discretely supported by elastic foundations

$$\delta = \lambda \frac{L^3}{EI} \tag{10}$$

where $\delta = y/Q$, y being the settlement y produced under the sleeper over which the load Q is placed (in other words, the inverse of the track stiffness without considering the contribution of the rail); L is the distance between the sleepers; and EI is the product of the elasticity modulus and the moment of inertia of the rail. For this case, the values for parameter δ corresponding to the different track sections are given by the model presented in Section 3. The parameter λ can therefore be obtained from Equation 9.

Upon this theory, when the wheel is situated directly above a sleeper, the rail deflection η_A is obtained as

$$\eta_A = \delta R_{A0} = \lambda \frac{L^3}{EI} \frac{1+3p}{3pq} Q \tag{11}$$

where R_{A0} is the reaction under that sleeper – that is, the part of the load Q which is transferred to the ballast (the rest of the load is supported among the adjacent sleepers) – and p and q are two parameters defined as

$$p = \sqrt{\left(\frac{1+48\lambda}{3}\right)}, \qquad q = \sqrt{\left(\frac{4}{3}+2p\right)} \tag{12}$$

When the wheel is placed at the centre of a sleeper bay, then the deflection under the adjacent sleepers $\eta_{A'}$, $\eta_{B'}$ becomes

$$\eta_{A'} = \eta_{B'} = \lambda \frac{L_3}{EI} \frac{1+3p}{3pq} Q \tag{13}$$

In order to find the total deflection under the wheel, it has to be added to $\eta_{A'}$ the deflection caused by a point load in a both-ends-fixed beam z_{CB1}, plus the deflection caused by the bending moments existing at the extremes A' and B', z_{CB2}. The first term is defined by

$$14.\quad z_{CB1} = \frac{QL^3}{48EI}$$

whereas the second term is given by

$$15.\quad z_{CB2} = \frac{M_{A'}L^2}{8EI}$$

with

$$16.\quad M_{A'} = \frac{1+2p-2q}{8q}QL$$

Then, the total deflection z_{CB} when the wheel is located at the centre of a sleeper bay is the sum of Equations 12, 13 and 14.

$$17.\quad z_{CB} = \eta_{A'} + z_{CB1} + z_{CB2}$$

In this sense, assuming the track to be in perfect condition, a wheel would describe a path which can be represented by the function

$$18.\quad z_s(s) = \frac{z_{CB}(s) - \eta_A(s)}{2}\sin\left(\frac{2\pi}{L}s\right)$$

In Equation 18, $z_{CB} = z_{CB}(s)$ and $\eta_A = \eta_A(s)$ because the deflections vary together with the track stiffness. This is the main factor responsible for the increase in the dynamic loads. In order to simplify the calculations, the variation of the vertical stiffness was discretised in two parts for the case of no transition zone and five parts for the case of placing a transition zone between the embankment and the structure. The different parts in which the vertical stiffness has been discretised have been chosen so they contain an entire number of sleeper bays, and the edges of such parts coincide with some points being placed directly over the sleepers, in which the rail profile achieves null amplitude according to Equation 18. In this way, the rail profile varies in amplitude while being a continuous and first-order derivable function throughout the evaluated length. Figure 13 shows the rail profile for the case of transition zone (Figure 13(a)) and no transition zone (Figure 13(b)), both with USP of 7500 kPa of elasticity modulus. Numeric data for the implementation of the dynamic model is shown in Table 3.

The actual rail profile z_a is obtained by superposition of the rail profile obtained with the static model z and the profile from Equation 18.

$$19.\quad z_a(s) = z(s) + z_s(s)$$

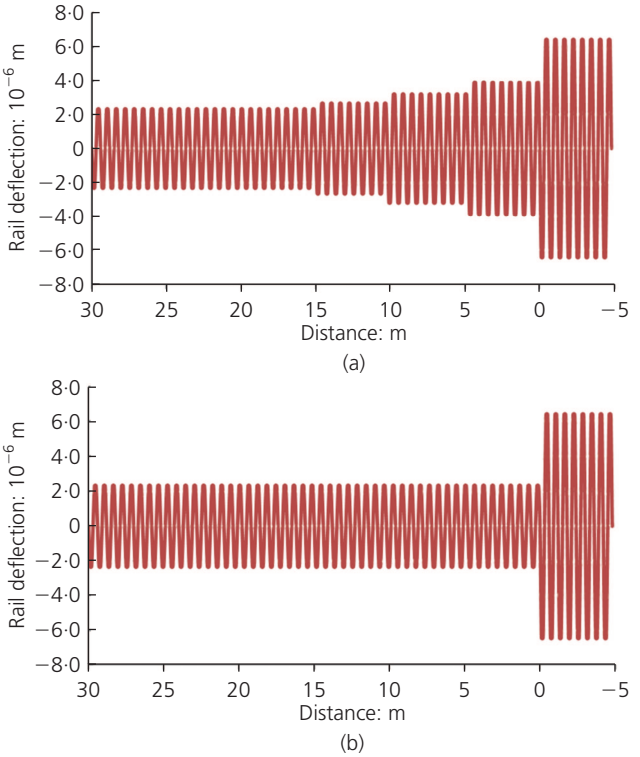

Figure 13. Rail profile obtained with the Unold–Dischinger–Lorente Nó method for the cases (a) with a transition zone and (b) without

This rail profile is input into the dynamic model shown in Equations 5. Since this set of equations is defined in the time domain, the change of variable $s = s_0 + Vt$ must be made, in which s_0 is the initial position of the train, V is the speed of the train and t represents time. Something analogous has to be done with the track vertical stiffness $k_1(s)$.

6. Analysis of the results

Figure 14 shows the vehicle body accelerations obtained with the dynamic model for the case of placing a transition zone and varying the elasticity modulus of the USP. The maximum value of acceleration is about 0·05 m/s^2 and is reached at the beginning of the structure. The rippled shape of the graph is due to the contribution of the parametric excitation, which is emphasised as the train reaches the structure, according to the Unold–Dischinger–Lorente de Nó theory. The sharp increase of the acceleration at the beginning of the simulation is caused by the initial boundary conditions shown in Equation 8 and usually happens in models solved by FDM. As can be seen, no appreciable difference is found for the different USP stiffness modulus values.

Figure 15 shows the analogous results of Figure 14 for the case with the embankment being directly in contact with the structure. The maximum value of accelerations is slightly lower than 0·15 m/s^2 and again is reached where the structure begins. It is interesting to

Track		
E	Young's modulus of rail	210 GN/m^2
I	Rail moment of inertia	$30{\cdot}06 \times 10^{-6}$ m^4
L	Distance between sleepers	0·6 m
Train		
Q	Wheel–rail static load	79·919 kN
m_3	Car body mass	6755 kg
m_2	Bogie frame mass	650 kg
m_1	Wheelset mass	750 kg
k_3	Secondary suspension stiffness	300 kN/m
k_2	Primary suspension stiffness	2200 kN/m
k_1	Track global stiffness	variable
c_3	Secondary suspension damping	50 kN s/m
c_2	Primary suspension damping	30 MN/m
c_1	Track global damping	0 kN s/m

Table 3. Numerical values for the calculation of rail deflection due to the parametric excitation and the train–track interaction dynamic model

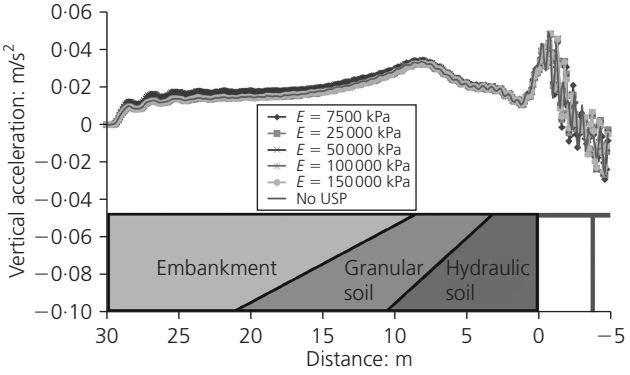

Figure 14. Car body accelerations for a train running from the embankment to the structure, with transition zone being considered

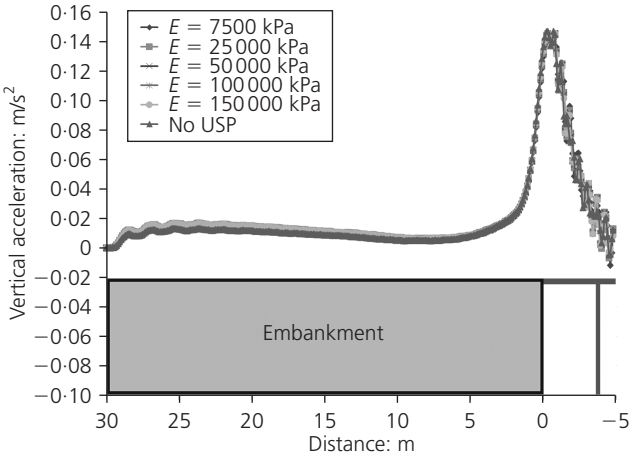

Figure 15. Car body accelerations for a train running from the embankment to the structure, no transition zone

compare this result with the maximum permitted accelerations. For various railway administrations such maximum accelerations are

$a_{v,max} = 0{\cdot}79$ m/s^2 – Norms FS (Italy)
$a_{v,max} = 0{\cdot}26$ m/s^2 – Norms DB (Germany).

As can be seen, the value of 0·15 m/s^2 is relatively close to the maximum given by the German Norm. Since for this simulation tracks in perfect conditions were assumed, these maximum values could easily be exceeded if the track had some small irregularities, which is the most common situation.

Again, the rippled shape is produced by the parametric excitation, and the initial increment of the acceleration values is the result of the boundary conditions reflected in Equation 8. In reference to the USP modulus, again no appreciable difference is found.

Finally, Figures 16 and 17 show the dynamic wheel load in terms of overload and unload percentages with respect to the static value for the cases with a transition zone and without, respectively. This force is given by the dynamic model described in Section 5 by applying the formula

$$F(t) = \sum_{i=1}^{3} m_i \ddot{x}_i + g \sum_{i=1}^{3} m_i \quad (20)$$

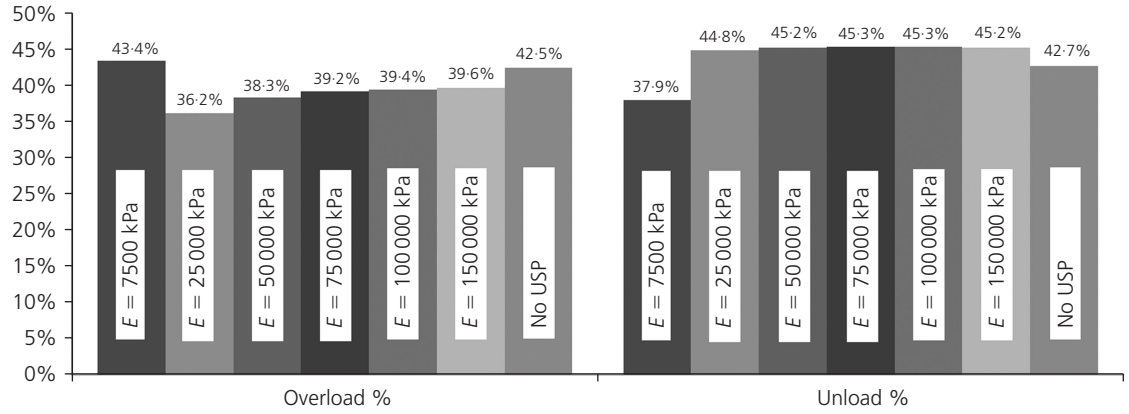

Figure 16. Overload and unload increments in respect of the static wheelset load, with transition zone

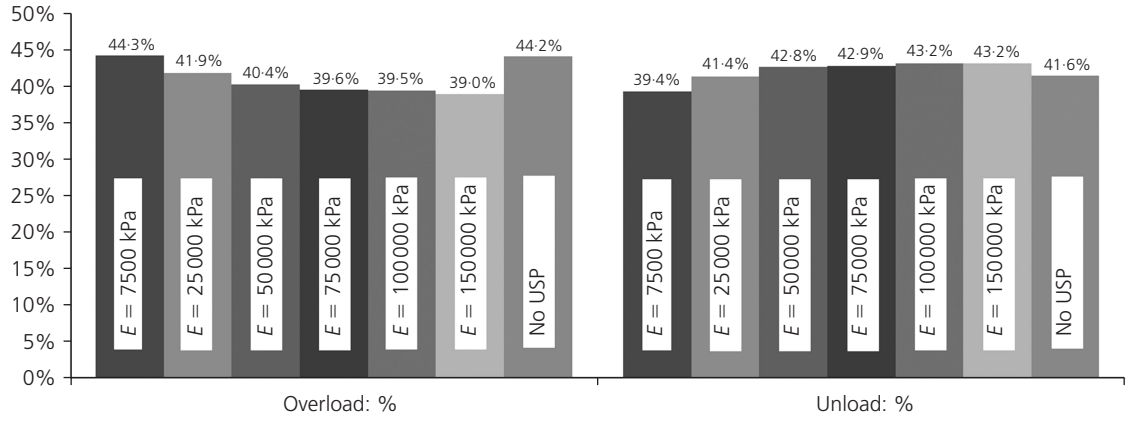

Figure 17. Overload and unload increments in respect of the static wheelset load, no transition zone

where the first part of the right-hand term is the contribution of the different masses affected by their respective accelerations and the second part becomes the static load, g being the acceleration of gravity.

Once again, no significant difference with the USP stiffness variation is found. The small variations which can be perceived are mainly produced by the initial boundary conditions and numerical errors. In this case, there is no significant difference between using and not using a transition zone. The reason for this may be found by looking at Figure 13. It can be seen in Figure 13(a) that the difference in amplitude between the last part and the adjacent part, each with constant stiffness (from $s \in [5, 0]$ and $s \in [0, -5]$), is bigger than the difference in amplitude among the previous parts. This shows that, even placing a transition zone between the embankment and the structure, the change in the stiffness is not homogeneously achieved and the larger stiffness variations occur in the few metres next to the structure. The rail profile shown in Figure 7 also supports this idea. This produces dynamic loads that are increased in the same proportions as if there were no transition zone.

Nevertheless, this result is not conclusive since the stiffness discretisation is not sufficiently accurate. In order to obtain more precise results, a higher level of resolution in terms of stiffness discretisation might be necessary.

7. Conclusion

In this paper, the effect of installing USPs in transition zones has been studied. Results show that USPs have no significant influence on the deflections and stresses produced in the infrastructure below ballast level, even when varying some properties, such as the elastic modulus, the pad thickness, or the pads' location in relation to the structure.

It is important to remark that the dynamic model must reflect both the track deformation caused by the quasi-static load and that produced by the parametric excitation. This is so because, whereas the first deformation particularly influences the vehicle

body accelerations, the second one plays its major role on the dynamic loads. Under these conditions, the paper further demonstrates that USPs should not be used to replace transition regions since they are not able to smooth sufficiently the vertical accelerations on the train as it passes on to the structure.

However, since USPs do not negatively affect the railway infrastructure, they are suitable for consideration from other points of view, such as ballast preservation.

REFERENCES

Adif (Administrador de Infraestructuras Ferroviarias) (2008) *Instrucciones Generales para los Proyectos de Plataforma IGP.* Adif, Madrid, Spain (in Spanish).

Baeza L, Roda A and Nielsen JCO (2006) Railway vehicle/track interaction analysis using a modal substructuring approach. *Journal of Sound and Vibration* **293(1–2)**: 112–124.

Burrow M, Teixeira P, Dahlberg T and Berggren E (2010) Track stiffness considerations for high speed railway lines. In *Railway Transportation: Policies, Technology and Perspectives* (Scott NP (ed.)). Nova Publishers, Hauppauge, NY, USA, 303–354.

Dahlberg T (2010) Railway track stiffness variations – consequences and countermeasures. *International Journal of Civil Engineering* **8(1)**: 1–12.

Dischinger F (1942) Der Durchlaufende träger und rahmen auf elastisch senkbaren und stützen. *Der Bauingenieur* **23**: 15–27 (in German).

Esveld C (2001) *Modern Railway Track*, 2nd edn. Dior Zwarthoed-van Nieuwenhuizen, Delft, the Netherlands.

Gallego I and López Pita A (2009) Numerical simulation of embankment–structure transition design. *Proceedings of the Institution of Mechanical Engineers. Part F: Journal of Rail and Rapid Transit* **223(4)**: 331–343.

Hanson CE and Singleton JHL (2006) Performance of ballast mats on passenger railroads. Measurement vs. projections. *Journal of Sound and Vibration* **293(4)**: 873–877.

Hyslip JP, Li D and McDaniel CR (2009) Railway bridge transition case study. In *Bearing Capacity of Roads, Railways and Airfields* (Tutumluer E and Al-Qadi IL (eds)). CRC Press, Leiden, the Netherlands, vol. 1 and 2, pp. 1341–1348.

Johansson A, Nielsen JCO, Bolmsvik R, Karlström A and Lundén R (2008) Under sleeper pads – influence on dynamic train–track interaction. *Wear* **265(9–10)**: 1479–1487.

Kaewunruen S and Remennikov AM (2006) Sensitivity analysis of free vibration characteristics of an in situ railway concrete sleeper to variations of rail pad parameters. *Journal of Sound and Vibration* **298(1–2)**: 453–461.

Lei X and Mao L (2004) Dynamic response analyses of vehicle and track coupled system on track transition of conventional high speed railway. *Journal of Sound and Vibration* **271(3–5)**: 1133–1146.

Li ZG and Wu TX (2009) On vehicle/track impact at connection between a floating slab and ballasted track and floating slab track's effectiveness of force isolation. *Vehicle System Dynamics* **47(5)**: 513–531.

Lorente de Nó C (1980) Viga continua sobre apoyos elásticos. In *Geotectnia y Cimientos III* (Jiménez-Salas JA (ed.)). Rueda. Madrid, Spain, Ch. 1.1.7 (in Spanish).

Maes J, Sol H and Guillaume P (2006) Measurements of the dynamic railpad properties. *Journal of Sound and Vibration* **293(3–5)**: 557–565.

Melis M (2008) *Apuntes de introducción a la dinámica vertical de la vía y a las señales digitales en ferrocarriles*. UPM. Madrid, Spain (in Spanish).

Ministerio de Fomento (1999) *Recomendaciones para el proyecto de plataformas ferroviarias*. Centro de Publicaciones de la Secretaría General Técnica del Ministerio de Fomento, Madrid, Spain (in Spanish).

Profidillis V (1983) *La Voie Ferrée et sa Fondation Modelisation Mathematique*. Doctoral thesis, École Nationale des Ponts et Chausées, Paris, France (in French).

Prud'Homme MA (1970) La voie. *Revue Générales des Chemins de Fer* **1(1)**: 52–72 (in French).

Puy J (1985) *Algoritmos numéricos en Pascal*. Servicio de Publicaciones de la ETSI Caminos, Madrid, Spain (in Spanish).

Ülker-Kaustell M, Karoumi R and Pacoste C (2010) Simplified analysis of the dynamic soil–structure interaction of a portal frame railway bridge. *Engineering Structures* **32(11)**: 3692–3698.

Unold G (1925) *Statik für den Eisen- und Maschinenbau*. Springer-Verlag, Berlin, Germany (in German).

Wang J, Zeng X and Gasparini DA (2008) Dynamic response of high-speed rail foundations using linear hysteretic damping and frequency domain substructuring. *Soil Dynamics and Earthquake Engineering* **28(4)**: 258–276.

Wettschureck R and Kurze UJ (1985) Erschütterungen in der Umgebung von flach liegenden Eisenbahntunneln im Vergleich mit freien Strecken. *Acustica* **58(3)**: 170–176 (in German).

Wu TX and Thompson DJ (2004) On the parametric excitation of the wheel/track system. *Journal of Sound and Vibration* **278(4–5)**: 725–747.

WHAT DO YOU THINK?

To discuss this paper, please email up to 500 words to the editor at journals@ice.org.uk. Your contribution will be forwarded to the author(s) for a reply and, if considered appropriate by the editorial panel, will be published as a discussion in a future issue of the journal.

Proceedings journals rely entirely on contributions sent in by civil engineering professionals, academics and students. Papers should be 2000–5000 words long (briefing papers should be 1000–2000 words long), with adequate illustrations and references. You can submit your paper online via www.icevirtuallibrary.com/content/journals, where you will also find detailed author guidelines.